Integrated Optical Interferometric Biosensors based on Microelectronics Technology for Biosensing Applications

F. Prieto[1], B. Sepúlveda[1], A. Calle[1], A. Llobera[2], C. Domínguez[2] and L.M. Lechuga[1]
Biosensors Group. Centro Nacional de Microelectrónica ([1]IMM/[2]IMB)-CNM.CSIC.
Isaac Newton 8 (PTM), 28760 Tres Cantos, Madrid (Spain)
e-mail: borja@imm.cnm.csic.es http://www.imm.cnm.csic.es/biosensores/home.html

Summary. *Integrated optical sensors have reached a great importance during last years since they can be used for the direct detection of biomolecular interactions. Moreover, Silicon microelectronics technology allows mass production as well as the fabrication of microsystems by hybrid integration of sources, sensors, photodetectors and CMOS electronics.*
For the fabrication of an evanescent field sensor with an integrated Mach-Zehnder interferometric (MZI) configuration, the optical waveguides must verify two main characteristics: monomode behaviour and high surface sensitivity. In this paper we present the development of a MZI sensor based on two different optical waveguides: TIR (Total Internal Reflection) and ARROW (Antiresonant Reflecting Optical Waveguides). The advantages of both structures are discussed and experimental results of the devices are presented.

Keywords: evanescent field sensor, MZI, biosensor
Subject category: 5 (Biosensors)

1. Introduction

Sensors based on integrated optics are acquiring great significance due to its high sensitivity, mechanical stability, possibility of miniaturisation and mass production [1]. These devices are based on evanescent field sensing: although light is confined within the core of the waveguide, there is a part of the guided light that travels through a region that extends outward, approximately a hundred nanometers, into the media surrounding the waveguide, so its field can interact with the environment. Therefore, a biomolecular interaction between a receptor molecule, previously deposited on the waveguide surface, and its complementary analyte produces a change in the refractive index at the sensor surface that induces a variation in the optical properties of the guided light via the evanescent field.

Among the different measurement configurations (grating coupler [2], resonant mirror [3],...) to detect this variation, we have chosen an interferometric method based on the Mach-Zehnder Interferometer (MZI) due to its higher sensitivity [4]. In a MZI [5], a phase shift between the sensing and the reference arm is induced by the biomolecular reaction that causes an intensity modulation at the sensor output.

For sensing applications, the optical waveguides that form the MZI sensor must verify two conditions: monomode behaviour and high surface sensitivity. In this work we present the development of a Mach-Zehnder interferometer sensor based on two different optical waveguides. Single-mode optical waveguides based on Total Internal Reflection (TIR) have a very high surface sensitivity [6] but present some drawbacks: the reduced core dimensions for monomode behaviour (thickness of hundreds nanometers and rib depths of few nanometers) implies a technological disadvantage for mass production and large insertion losses when coupling light with single-mode optical fibres (with a core thickness of several micrometers). To overcome these difficulties we propose the use of Antiresonant Reflecting Optical Waveguides (ARROW) [7]. Monomode behaviour for these waveguides can be achieved with core dimensions in the order of micrometers and, therefore, we eliminate the difficulty in the fabrication of TIR waveguides. Moreover, the larger core dimensions implies lower insertion losses for end-fire coupling. The main disadvantage of this structure is the lower surface sensitivity when compared with TIR waveguides.

2. MZI sensor configuration

In the integrated version of a Mach-Zehnder interferometer, an input optical waveguide is split into two arms, which, after a certain distance, recombine again in an output optical waveguide [5] (see Fig.1). The sensor is completely covered with a protective layer and only in one of the arms, a sensor area of length L is opened to bring into contact the waveguide and the

environment. When there is a change in the properties of the surrounding medium (i.e. refractive index), light travelling in the sensor arm will experience a phase shift in comparison with guided light in the other branch (reference arm). At the output optical waveguide, interference between light coming from both arms will be observed:

$$I \propto \left[1 + V \cdot \cos\Delta\Phi\right] \qquad (1)$$

where $\Delta\Phi = (\Phi_r - \Phi_s)$ is the phase shift between guided modes in the reference and sensing arm:

$$\Delta\Phi = \frac{2\pi}{\lambda} \cdot L \cdot \Delta N \qquad (2)$$

L is the length of the sensor area, λ is the wavelength and ΔN is the change in the effective refractive index produced by the variation in the properties of the outer medium. The visibility factor (V) gives the contrast of the interference signal (difference between the maximum and minimum intensity) and depends on the coupling factor of the divisor and on the propagation losses of the guided mode in the interferometer arms. To obtain a maximum visibility factor it is important to design a divisor or Y-junction with a coupling factor of 3 dB, that is, input light is equally divided in each branch of the interferometer. Moreover, propagation losses in the sensor and reference arm should be identical.

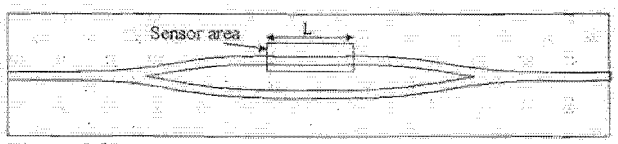

Fig. 1: MZI scheme

With these considerations, several MZI configurations were designed varying the Y-junction parameters. All the devices are symmetric with two different divisor shapes: in the first case the Y-junction is formed with straight arms and opening angle of 1°. In the second case, the divisor is shaped with circular bends with radii of 5, 20 and 80 mm. In all cases, the separation between the sensor and reference arms is of 100 μm to avoid coupling between modes travelling through both branches. In one arm, a sensor area with different lengths (6, 10, 15 and 20 mm) is created. The total length of the device is 35 mm.

3. Optical waveguides for sensing applications

The optical waveguides that will form the MZI must verify two conditions: monomode behaviour and high surface sensitivity. We have developed a MZI sensor based on two different types of optical waveguides: TIR and ARROW structures. For the fabrication of these waveguides we have used a Silicon CMOS compatible process [8].

The TIR waveguide is a three-layer structure in which the optical confinement of light is produced by total internal reflection at the interfaces of the core layer and the surrounding media (see Fig. 2a). The materials used for the fabrication of these structures are silicon oxide for the cladding (n_{clad} = 1.46) and silicon nitride for the core (n_{core} = 2.00). Single-mode behaviour for this configuration is obtained with core thickness in the order of hundreds of nanometers (100-300 nm) and rib depths of only a few nanometers (2-5 nm).

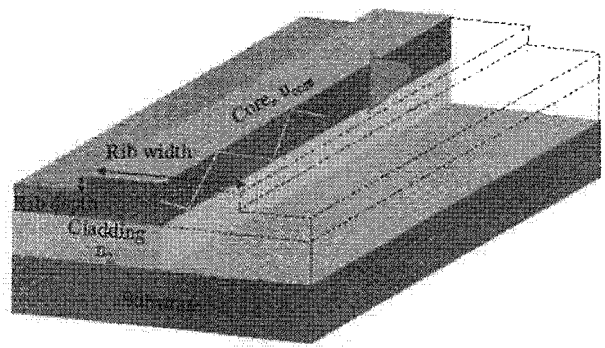

Fig. 2a: TIR waveguide configuration

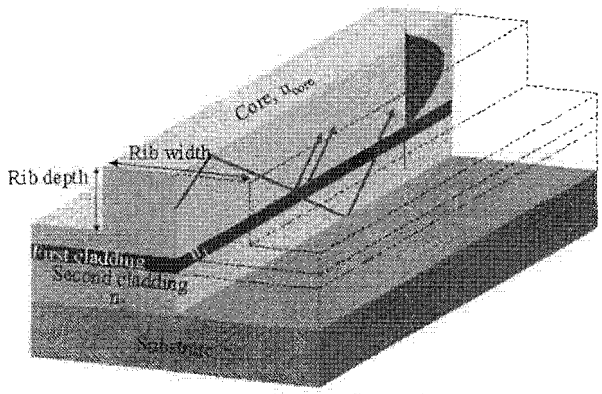

Fig. 2b: ARROW waveguide configuration

As we mentioned above, TIR waveguides for sensing applications present some drawbacks concerning the reduced dimensions of the core. To overcome these difficulties, we have proposed the use of optical waveguides based on the ARROW structure. In these waveguides, light is confined in the core by total internal reflection at the outer medium-core interface and by antiresonant reflection at the interference cladding underneath the core [9] (see Fig. 2b). The materials used for the fabrication of these structures are silicon oxide for the core and second cladding and silicon nitride for the first cladding. With this configuration, monomode behaviour is obtained with core thickness in the order of several micrometers (2-4 μm) and rib depths of few micrometers (60% of the core thickness). These dimensions are compatible with the diameter of

commercial optical fibers and, therefore, insertion losses are lower than for TIR waveguides. Moreover, the core dimensions also imply advantages in the fabrication processes.

However, surface sensitivity for the ARROW structure is two orders of magnitude lower than for TIR waveguides [7]. As it has been shown previously [10, 11], coating the core surface of the ARROW structure with a high refractive index thin layer can enhance surface sensitivity. For overlay thickness of some tens of nanometer (35-40nm) sensitivity is increased more than one order of magnitude and, with this configuration, the ARROW sensitivity differs only a factor 4 compared to surface sensitivity for TIR waveguides (see Figure 3).

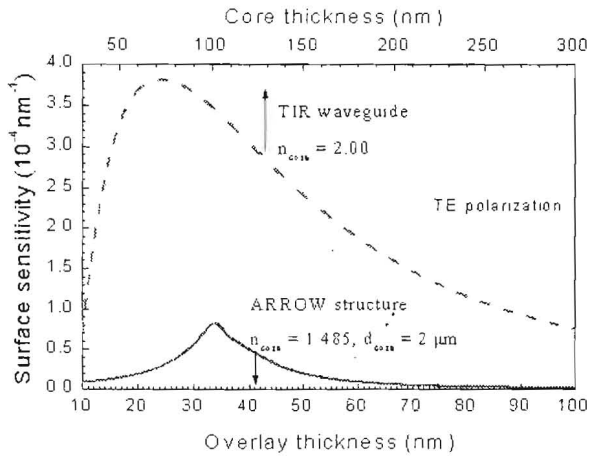

Fig 3. Comparison of surface sensitivity for the ARROW (solid line) and TIR (dashed line) structures (TE polarization).

3.1. Fabrication of the devices

The fabrication of the devices is performed on our Clean Room facilities using a CMOS compatible process. The scheme for the fabrication of ARROW structures is shown in Figure 4. The general structure is a substrate of Si, a 2 μm SiO_2 second cladding layer of refractive index 1.46, made by thermal oxidation of the Silicon substrate (see Figure 4 (a)), a 0.3 μm Si_3N_4 first cladding layer of refractive index 2.00, deposited using Low Pressure Chemical Vapour Deposition (LPCVD) at 800 °C (Figure 4 (b)) and a 2-4 μm SiO_x core, with refractive index ranging from 1.46-1.9 (depending on x), deposited by Plasma Enhanced Chemical Vapour Deposition (PECVD) at 300 °C (Figure 4 (c)). The technology of growing non-stoichiometric silicon oxide by PECVD has been developed previously in our group [12]. To obtain monomode lateral confinement of light, a rib structure with a depth of 60% of the core thickness and a width of 4-7 μm was defined by dry Reactive Ion Etching (RIE). Using this technique, the Mach-Zehnder configuration was defined on the core layer (Figure 4 (d)). On the top of the interferometer, a protective Silicon Nitride layer of 0.12 μm was deposited (Figure 4 (e)). Finally, the structure was covered with a silicon oxide layer of 2 μm (Figure 4 (f)). In one of the arms (sensor arm) the SiO_2 layer was etched in an area of 100 μm wide and 6-20 mm large in order to bring into contact the waveguide and the environment (Figure 4 (g)). Finally, the sensors are cut in individual pieces and polished for light coupling by end-face.

The fabrication process for the devices based on the TIR structure is similar to the one described above. In this case, the fabrication only involves the deposition of three layers: a 2 μm SiO_2 cladding layer of refractive index 1.46, grown by thermal oxidation of the Silicon substrate; the silicon nitride core layer (n_{core} 2.00) deposited by LPCVD with a thickness of 250 nm. After the definition of the MZI structure by RIE (rib depth = 3 nm), a 2 μm silicon oxide protective layer (n = 1.46) is deposited by PECVD.

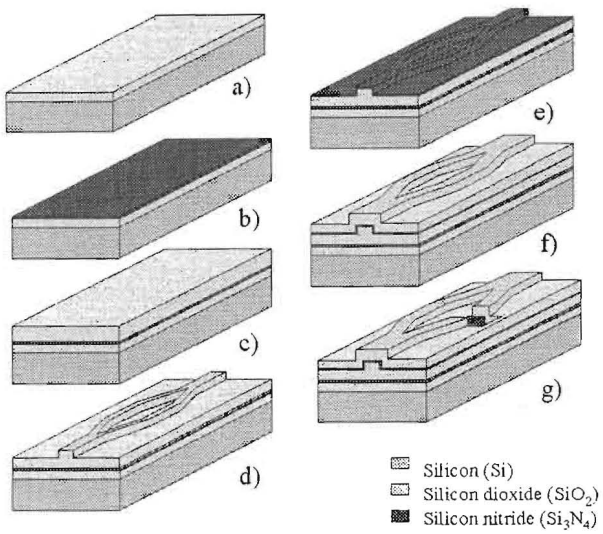

Figure 4. Fabrication process for the ARROW structure: a) SiO_2 second cladding growth by Thermal Oxidation; b) Si_3N_4 first cladding deposited by LPCVD; c) SiO_x core deposited by PECVD; d) definition of the sensor structure by RIE; e) Si_3N_4 overlay deposited by LPCVD; f) SiO_x protection layer deposited by PECVD; g) opening of the sensor area by RIE.

4. Experimental evaluation

For the experimental evaluation, light from a He-Ne laser (λ=632.8 nm) is coupled to a single-mode optical fibre (3.8 μm core diameter) using a microscope objective (40 x). The end of the monomode fibre is placed in front of the waveguide rib face to couple light into the sensor (end-fire coupling). Light is collected by a multimode optical fibre (50 μm core diameter) connected to a PIN silicon photodiode. We use precise translation stages for the accurate alignment of all the

components. A synchronous detection scheme is used with the aid of a lock-in amplifier and a light chopper.

The sensor is being developed for the detection of biochemical interactions between a receptor molecule and its complementary analyte. The effect of this reaction is comparable to a change of the bulk refractive index of the outer medium. Therefore, the use of solutions with different refractive indexes is useful for studying the sensor sensitivity. Several solutions were prepared with different glucose concentrations in water, with refractive indexes varying from 1.3325 to 1.4004 (± 0.0002), as determined by an Abbe refractometer operating at 25 °C. A flow cell mechanised in Teflon (with a channel width of 3 mm, a depth of 100 µm and a length of 15 mm) is clamped onto the interferometer and a flow injection system is used to deliver the glucose solutions into the sensor area.

4.1. ARROW-MZI sensor

Next, results with the MZI sensors fabricated with the ARROW structure are presented. Using as a reference the refractive index of deionised (DI) water (1.3325), different glucose solutions with varying refractive indexes were introduced alternatively, as it is shown in Figure 5. With these measurements, a calibrating curve was evaluated where the phase response of the sensor is plotted versus the variation in the refractive index. Figure 6 shows these calibrating curves for four different MZI sensors using TE polarization. For a sensor with a core thickness of 4 µm and the overlay thickness of 120 nm (solid circle in Fig. 6) sensitivity is very low, as theory predicts [7]. However, if the overlay thickness is decreased to some tens of nanometers, i.e. 39 nm (solid square in Fig. 6), sensitivity is enhanced more than an order of magnitude [10]. In this case, the detection limit for the refractive index variation is $\Delta n_{o,min} = 1 \cdot 10^{-3}$ ($\Delta N = 1 \cdot 10^{-5}$).

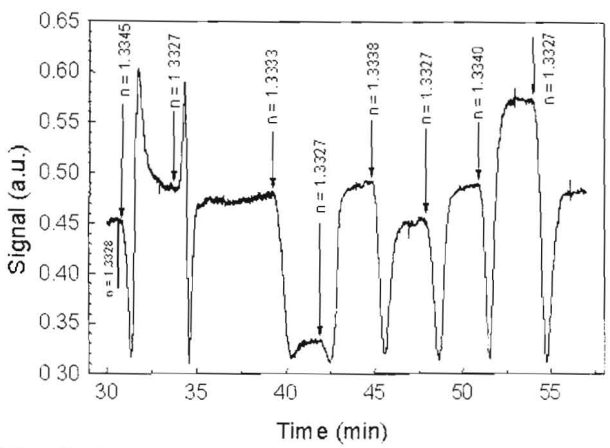

Fig. 5. Sensor response for a change of the refractive index in the sensor area. Variation for glucose solutions with different refractive indexes. TE polarization.

Sensitivity can also be increased if the core thickness diminishes because the guided mode is less confined within the core [7]. For a sensor with 3 µm of core thickness (open square in Figure 6) the refractive index detection limit is one order of magnitude higher than before ($\Delta n_{o,min} = 1 \cdot 10^{-4}$ ($\Delta N = 2 \cdot 10^{-5}$)).

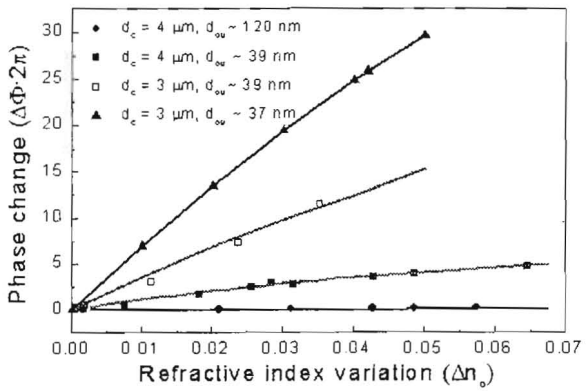

Fig. 6. Calibrating curves for the MZI-ARROW sensor with different waveguide structures (see the inset) (TE polarization).

Finally, as it is shown in Figure 3, for small variations of the overlay thickness, sensitivity can be increased significantly. A variation of only 2 nm in this overlay (37 nm, solid triangle in Figure 6) implies a sensitivity increment of almost one order of magnitude. In this case, the maximum sensitivity obtained is $\left(\frac{d\Delta\Phi(2\pi)}{dn}\right)_{ARROW} = 481$, which corresponds to a minimum detectable refractive index variation of $\Delta n_{o,min} = 2 \cdot 10^{-5}$ ($\Delta N = 1 \cdot 10^{-6}$).

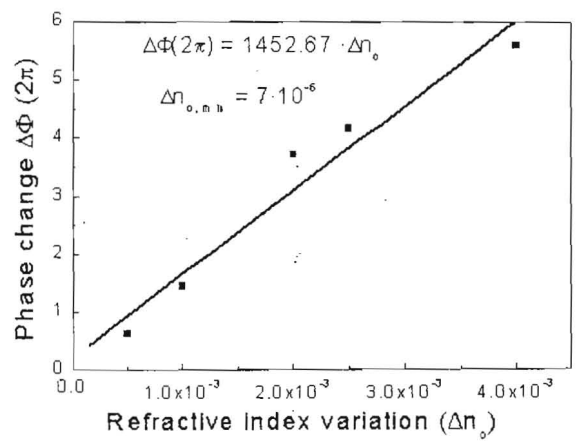

Fig. 7. Calibration curve for the MZI-TIR sensor. Core thickness of 250 nm, TM polarization.

4.2. TIR-MZI sensor

The same type of measurements was performed with a MZI sensor fabricated with the TIR structure. We selected a sensor with a core thickness of 250 nm and a rib width of 3 nm. Results for TM polarization are shown if Figure 7. Sensitivity for the MZI-TIR sensor ($\left(\frac{d\Delta\Phi(2\pi)}{dn}\right)_{TIR}$ = 1453) is a factor 3 higher than for the sensor based on the ARROW structure. This implies a lower detection limit of $\Delta n_{o,min} = 7 \cdot 10^{-6}$ ($\Delta N = 7.5 \cdot 10^{-7}$).

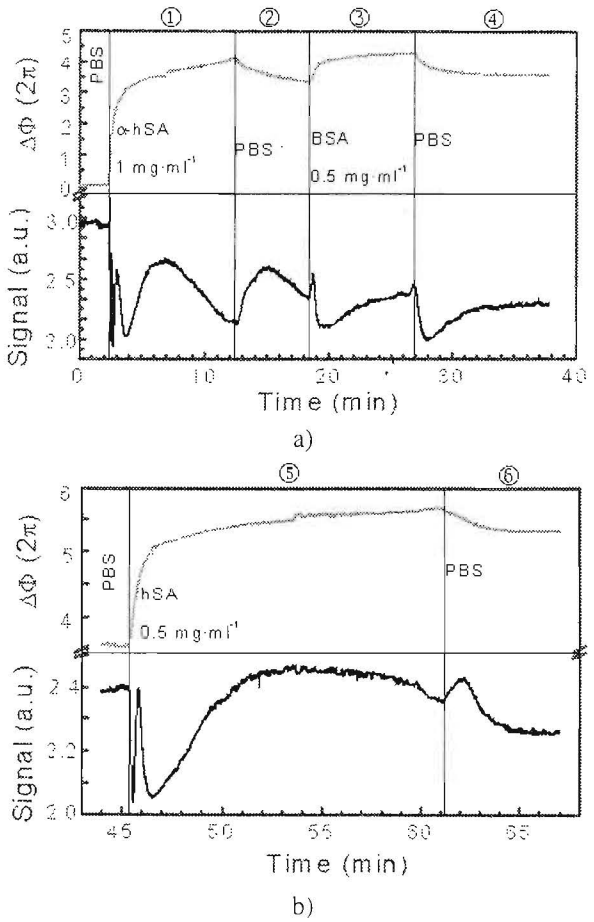

Fig. 8. Signal response (TE polarisation) of the MZI-ARROW sensor to the antigen/antibody α-HSA/HSA immunoreaction. 1) Physical adsorption of the α-HSA antibody. 2) Rinsing with PBS. 3) Blocking with BSA. 4) Rinsing with PBS. 5) Immunoreaction with the antigen HSA. 6) Rinsing with PBS.

5. Biosensor applications

As an example of biosensing application we have used the sensor for the detection of the immunoreaction antibody-antigen α-HSA/HSA (*Human Serum Albumin*, Sigma A0433). The measurements have been performed with a MZI-ARROW sensor with 3 μm of core thickness, an interaction length of 15 mm and an overlay thickness of 37 nm.

Measurements are performed in phosphate buffered saline (PBS), with a pH of 7.35, at room temperature and maintaining a low flow rate (20 μl/min). Initially, a concentration of $6.7 \cdot 10^{-6}$ M (1mg· ml^{-1}) human serum albumin antibody (α-HSA) is introduced in the sensor area. Figure 8a shows the response of the sensor to the physical adsorption of the antibodies, that correspond to a net phase change of $\Delta\Phi = 4.2 \cdot 2\pi$, equivalent to a surface coverage of 1.8 ng· mm^{-2}. After rinsing with PBS and blocking with BSA (bovine serum albumin), a concentration of $7.7 \cdot 10^{-6}$ M human serum albumin antigen (HSA) is flowed through the sensor, giving a net phase change of $\Delta\Phi = 2 \cdot 2\pi$ (Figure 8b) due to the immunoreaction.

6. Conclusions

We have developed an evanescent field sensor based on Silicon microelectronics technology. It makes use of an integrated MZI configuration fabricated with two different waveguide structures: TIR and ARROW. The main features of these waveguides must be monomode behaviour and high surface sensitivity. To achieve these characteristics for ARROW we employ a modified structure in which the core is overcoated with a high refractive index thin layer. To obtain monomode behaviour, the parameters of the waveguide must be carefully chosen. We have presented experimental results of a MZI sensor based on the two waveguides working as a refractometer. For the MZI-ARROW sensor the lower refractive index detection limit is $\Delta n_{o,min} = 2 \cdot 10^{-5}$, while for the MZI-TIR sensor, this limit is a factor 3 lower ($\Delta n_{o,min} = 7 \cdot 10^{-6}$). Finally, we present a preliminary result of the MZI-ARROW sensor for biochemical applications.

References

[1] R. P. H. Kooyman and L. M. Lechuga, "Immunosensors based on total internal reflectance," in *Handbook of biosensors and electronic noses*, E. Kress-Rogers, Ed. New York: CRC Press, 1997, pp. 169-196.

[2] K. Tiefenthaler, W. Lukosz, "Sensitivity of grating couplers as integrated-optical chemical sensors", *J. Opt. Soc. Am. B*, vol. 6, n. 2, pp. 209-220, 1989.

[3] R. Cush, J.M. Cronin, W.J. Stewart, C.H. Maule, J. Molloy, N.J. Goddard, "The resonant mirror: a novel optical biosensor for direct sensing of biomolecular interactions. Part I: principle of operation and associated instrumentation", *Biosen. and Bioelectron.*, vol. 8, pp. 347-353, 1993.

[4] W. Lukosz, "Principles and sensitivities of integrated optical and surface plasmon sensors for direct affinity sensing and immunosensing," *Biosen. Biolectron.*, vol. 6, pp. 215-225, 1991.
[5] R. Syms, J. Cozens, *Optical guided waves and devices*, Ed. McGraw Hill, Londres, 1992.
[6] E.F. Shipper, A.M. Brugman, C. Domínguez, L.M. Lechuga, R.P.H. Kooyman, J. Greve, "The realization of an integrated Mach-Zehnder waveguide immunosensor in silicon technology," *Sensors and Actuators B*, vol. 40, pp. 147-153, 1997.
[7] F. Prieto, A. Lobera, D. Jiménez, C. Domínguez, A. Calle and L.M. Lechuga, "Design and Analysis of Silicon Antiresonant Reflecting Optical Waveguides for Evanescent Field Sensors," *J. of Lightwave Technol.* vol. 18, pp. 966-972, 2000.
[8] Moreno, M., Garcés, I., Muñoz, J., Domínguez, C., Calderer, J., Villuendas F. & Pelayo, J. "CMOS Compatible ARROW Guides" Proc. of the 8th CIMTEC-World Ceramic Congress and Forum on New Materials, Advanced Materials in Optics, Electro-Optics and Communications Technologies, Firenza (Italy), pp. 465-472, 1995.
[9] Duguay, M.A., Kokubun, Y. & Koch, T.L. "Antiresonant Reflecting Optical Waveguides in SiO_2-Si Multilayer Structures" Applied Physics Letters, 22, pp. 892, 1986.
[10] F. Prieto, L.M. Lechuga, A. Calle, A. Lobera and C. Domínguez, "Optimixed Silicon AntiResonant Reflecting Optical Waveguides for Sensing Applications," *J. of Lightwave Technol.*, January 2001.
[11] G.R. Quigley, R.D. Harris and J.S. Wilkinson, "Sensitivity enhancement of integrated optical sensors by use of thin high-index films," *Applied Optics.*, vol. 38, no. 28, pp. 6036-6039, 1999.
[12] C. Domínguez, J. A. Rodríguez, F. J. Muñoz and N. Zine, "Plasma enhanced CVD silicon oxide films for integrated optic applications." *Vacuum*, vol. 52, pp. 395-400, 1999.